PHOTONICS Research

Time interval measurement with linear optical sampling at the femtosecond level

Dongrui Yu,[1] Ziyang Chen,[1,3] Xuan Yang,[2] Yunlong Xu,[2] Ziyi Jin,[2] Panxue Ma,[2] Yufei Zhang,[1] Song Yu,[2] Bin Luo,[2,4] and Hong Guo[1,5]

[1]State Key Laboratory of Advanced Optical Communication Systems and Networks, School of Electronics, and Center for Quantum Information Technology, Peking University, Beijing 100871, China
[2]State Key Laboratory of Information Photonics and Optical Communications, Beijing University of Posts and Telecommunications, Beijing 100876, China
[3]e-mail: chenziyang@pku.edu.cn
[4]e-mail: luobin@bupt.edu.cn
[5]e-mail: hongguo@pku.edu.cn

Received 26 June 2023; revised 19 September 2023; accepted 17 October 2023; posted 18 October 2023 (Doc. ID 498810); published 1 December 2023

High-precision time interval measurement is a fundamental technique in many advanced applications, including time and distance metrology, particle physics, and ultra-precision machining. However, many of these applications are confined by the imprecise time interval measurement of electrical signals, restricting the performance of the ultimate system to a few picoseconds, which limits ultrahigh precision applications. Here, we demonstrate an optical means for the time interval measurement of electrical signals that can successfully achieve femtosecond (fs) level precision. The setup is established using the optical frequency comb (OFC) based linear optical sampling (LOS) technique to realize timescale-stretched measurement. We achieve a measurement precision of 82 fs for a single LOS scan measurement and 3.05 fs for the 100-times average with post-processing, which is three orders of magnitude higher than the results of older electrical methods. The high-precision time interval measurement of electrical signals can substantially improve precision measurement technologies.

https://doi.org/10.1364/PRJ.498810

1. INTRODUCTION

High-precision time measurement has significant applications in various fields, including remote time synchronization [1–4] and precise navigation systems [5–8]. A prominent example is the research on numerous scientific experiments, where high-precision time measurement can directly limit the experimental performance, such as time-of-flight measurement in high-energy particle physics [9], dark matter detection and measurement of fundamental constants [10–16]. Specifically, high precision is always the ultimate goal of time measurement, and the progression of its technique can help overcome technical bottlenecks in precision measurement in relevant fields and can also bring about a breakthrough in discovering new areas of physics, such as particle physics and cosmology.

Traditional solutions to measure the time interval of electrical signals use electrical means [17–19]. They measured the equivalent voltage proportional to the time interval under test [9,20] or used the digital counting method to directly count the number of clock cycles [9,20–22]. The precision of the former method, with the order of hundred picoseconds (ps), is limited by the poor resolution of digital devices; the latter methods, with the help of the dual mixer time difference measurement technique, can achieve performance better than 0.1 ps [23]. However, such a sub-ps-level time interval measurement cannot satisfy the requirements of state-of-the-art precise implementations, such as gravitational wave detection and femtosecond (fs) level time frequency transfer. To support the rapidly growing precision requirement and the expanding directions of applications, researchers must urgently find a breakthrough approach for precision measurement.

Compared to traditional electrical techniques, optical frequency comb (OFC) based techniques offer a possibility for high-performance time frequency measurement because of their ultrahigh time resolution [24–27]; therefore, this technology enables high-precision time interval measurement. Remarkably, dual OFC based linear optical sampling (LOS) techniques have been extensively studied in many high-precision measurement fields. For example, fs-level remote time synchronization [1,28,29] and nanometer absolute distance measurement [30–33] have been achieved, showing the advantage of using optical means for precision measurement. However, the time interval measurement of electrical signals by optical methods faces numerous technical difficulties, such as the noise introduced by electro-optical conversion, the

precision of optical methods, the robustness and complexity of the optical system, and the capability of measuring irregular waveforms, which leads to challenges for high-performance and simple system design.

Here, we demonstrate an optical method for ultrahigh precision time interval measurement that measures two periodic electrical signals with fs-level precision, despite arbitrary waveforms. The electrical pulses under test were locked to the repetition frequencies of two OFCs to transfer the interval information from the electrical to the optical region. By introducing dual-comb LOS technology, we used a third OFC locked to one of the signals being tested to sample the two optical pulses, which in principle overcomes the limitation of electrical means. Because the carrier-envelope offset frequency does not need to be manually stabilized, the complexity of the entire system was significantly reduced. We showed that the precision of the time interval measurement of electrical pulses fell below 3.05 fs after LOS and post-processing. The findings demonstrate the feasibility of the fs-level time interval measurement of electrical pulses and provide support for ultrahigh-precision microwave applications.

2. RESULTS

A. Experimental Setup

A schematic diagram of the time interval measurement system is illustrated in Fig. 1(a). When measuring two input electrical periodic signals with arbitrary waveforms, traditional electrical methods are difficult to quantify with sufficient precision. For this reason, our proposed optical protocol performs four procedures to achieve better measurement precision: signal preprocessing, electrical-to-optical signal conversion (E-O conversion), LOS processing, and data acquisition and post-processing.

In the signal preprocessing phase, the system uses adjustable bandpass filters (BPFs) and frequency multipliers/dividers to obtain a single harmonic component of the input waveforms that equals integer multiples of 100 MHz for the subsequent process. Note that the phase time of every harmonic contains

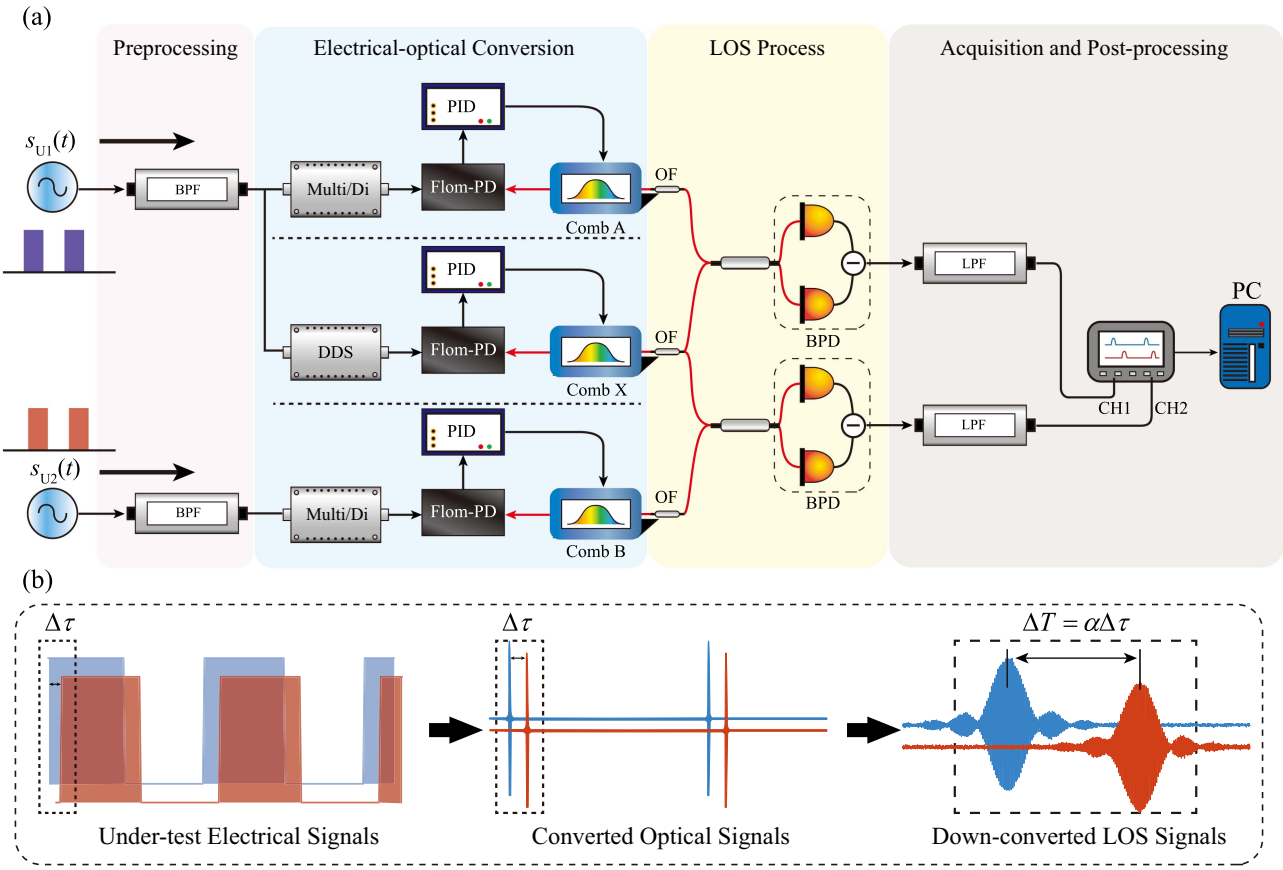

Fig. 1. Schematic of the time interval measurement setup. (a) Time interval measurement setup. The two band-pass filters (BPFs) in the preprocessing part filter a certain harmonic of the under-test pulses, which serve as the combs' reference after being multiplied, divided, or synthesized. The direct digital synthesizer (DDS) in the electrical-to-optical conversion part generates a sinusoidal wave with a slight frequency difference from its input signal. The repetition frequencies of three combs are phase-locked with the fiber-loop optical-microwave phase detector (FLOM-PD) and the PID. The outputs of combs A and B are sampled through LOS with comb X, and then detected and acquired by balanced photodetectors (BPDs) and an oscilloscope. The low-pass filters (LPFs) are used to isolate the final output. (b) Conversion of the under-test electrical pulses to the measured LOS signals. Through preprocessing and electrical-optical conversion, the signals are converted to two optical-frequency-comb signals, carrying the same time-interval information as the under-test signals. Through the LOS process, the optical signals are down-converted to two LOS signals in terms of the frequency, whose time intervals are amplified α times in comparison with the under-test signals.

the same information as the original electrical signal dose [34] (see the Appendix A). Measuring the time interval of the sine signal directly by electrical means leads to the precision of the ps level [35,36]. To overcome this limitation, in the E-O conversion process, we lock the repetition frequencies of two OFCs, namely comb A and comb B, to the previously obtained single harmonic signals using the fiber-loop optical-microwave phase detector (FLOM-PD) technique [37–39]. In our scheme, the 2 GHz harmonic of the signal being tested is obtained and used for phase locking, and the residual phase noise after phase locking was 8×10^{-14} at 1 s, as evaluated by the phase noise analyzer (Microchip Technology, 53100A). It ensures a standard deviation of less than 45 fs of the locking-induced noise of the time measurement.

In the optical domain, the system uses the state-of-the-art LOS technique to downconvert two comb signals to microwave combs with α times precision improvement (see the Appendix A). The key parameter $\alpha = f_r/\Delta f_r$ quantifies the stretch of time scale when using a local oscillator (LO) comb [comb X in Fig. 1(a)], with a slightly different frequency of Δf_r, to sample the measured OFC with a frequency f_r, yielding a microwave comb containing the time information of the measured OFC, but with higher precision. The frequency difference is achieved by a direct digital synthesizer (DDS). Here, we used two OFCs with a repetition frequency of 100 MHz as the measured OFCs (comb A and B) and an OFC with a repetition frequency of 100.001 MHz as the LO-OFC, which improved the time measurement precision by $\alpha = 10^5$ times. Note that the repetition frequencies of the combs are all adjustable with a temperature controller and a PZT, enabling them to be synchronized to the signals being tested for the subsequent process.

In the LOS process, the optical part is constructed with full polarization-maintaining fiber couplers and optical filters (OFs) with a central wavelength of 1550.12 nm and a bandwidth of 0.8 nm to prevent polarization-induced amplitude fluctuation. OFs are used not only to limit the OFCs' spectrum in the same band to obtain a stable and clear interference pattern but also to fulfill the Nyquist condition and to prevent spectrum overlapping [40]. The interference result is subsequently transformed into an electrical signal with balanced photodetectors (BPDs, Thorlabs, PDB450C) for the convenience of data acquisition and processing. Therefore, the conversion process can be summarized by first converting the electrical signals being tested to optical signals and then downconverting to the microwave LOS signals using the LOS technique, as illustrated in Fig. 1(b). In the whole process, to ensure the long-term stability of the system, we shortened the pigtails of commercial wavelength division multiplexer (WDM) devices, couplers, and other optical components and directly fused them together. We also kept the electrical cables as short as possible and implemented temperature control in the detection section to minimize the impact of internal path variations on the time measurements. The upper and lower branches of the system have a baseline delay for not precisely matching the path length, while it is calibrated before conducting the measurements.

The acquisition part contains two electrical low-pass filters (81 MHz) to obtain the frequency components introduced by the beating OFCs, and an oscilloscope (OSC, Rigol, MSO8204) is used to simultaneously acquire the data from two channels. The duration of an LOS signal in our experiment was approximately 4 μs. To fit the envelope of the LOS signal accurately, we expected at least 100 points in the pulse duration. This means that the sampling rate was expected to be over 100 points/4 μs = 25 MHz. A higher sampling rate will improve the resolution of the LOS signal (see the Appendix A), while also increasing the data processing cost. To balance the LOS signal precision and the processing speed, we set the sampling rate to 500 MHz in our experiment. A screen containing a set of the LOS waveforms is shown in Fig. 2, where two input channels of the OSC are simultaneously acquired and then delivered to the computer. These two signals contain time information of the input electrical signals, but with higher measurement precision. The timescale of the downconverted LOS signal is at the microsecond level, which can be easily acquired and processed using digital signal processing techniques, compared to the timescale of tens of picoseconds level with direct measurement. The data processing procedure is given in the Appendix A.

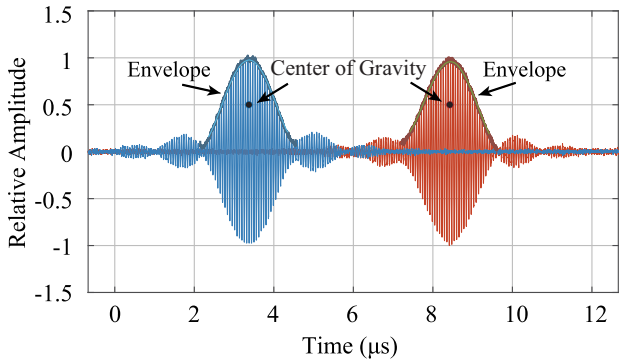

Fig. 2. Processing of the down-converted LOS signal by the envelope calculation and localization (i.e., center finding). The process is achieved by first fitting the signal's envelope and then calculating its center of gravity.

B. Measurement Precision

In our experiment, we assessed the precision of the time interval measurement system by generating the test signal by power-splitting a single 100 MHz square wave produced by an arbitrary waveform generator (AWG, Keysight, M8195A). As explained in Section 2.A, we applied filtering to isolate the first harmonic of the signals, which were then multiplied to 2 GHz. These resulting signals served as the references for comb A and comb B, respectively. Hence, the time interval of two square waves under test was transformed into the measurement of two downconverted LOS signals. In our scheme, we measured the interval by calculating the LOS envelopes' center of gravity, as shown in Fig. 2, and the calculated result is shown in Fig. 3(a). With continuous acquisition, the time interval could be displayed and plotted in real time. The black circles stand for the raw measured data, with the average value being −50.15 ps and the standard deviation being 83 fs. To further improve the precision, we also optimized the system's performance with a Kalman filter in real time. The red dots stand for the processed

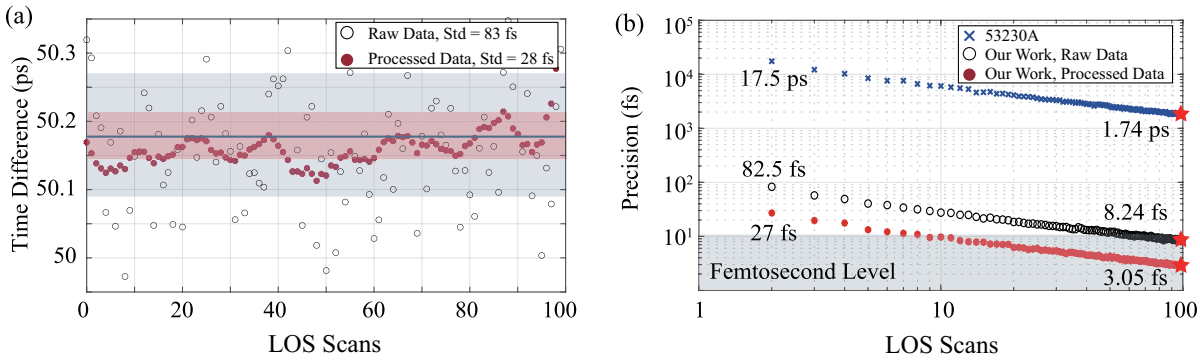

Fig. 3. Measurement results of system's precision. (a) Measurement results of the time difference. Black circles represent raw data, while red points represent data processed with the Kalman filter. (b) Measurement precision of the data. Blue crosses indicate the precision of a commercial time-interval counter (Keysight, 53230A). Black circles represent the precision of our work with raw data, while red points represent the precision of our work with processed data.

data with the Kalman filter, with the standard deviation being 28 fs.

To further reduce the system noise, we also considered averaging the sampling results to obtain the optimized results. Here, we used the standard error of the mean (SEM) to estimate the precision after averaging, given by

$$\mathrm{SEM} = \sigma(T)/\sqrt{n}, \tag{1}$$

where σ represents the standard deviation of the data, and n is the number of scans of the LOS measurement. We estimated the system's performance after averaging, and the precision is shown in Fig. 3(b). As the scanning number increased, the sample mean gradually approached the expectation value with a slope of tangent of $-1/2$, and the measurement precision reached 8.24 fs with an average of 100 raw data and 3.05 fs with an average of 100 Kalman-filtered data.

Furthermore, our scheme can measure the time interval of periodic signals with arbitrary waveforms. To demonstrate this, we generated sine waves, square waves, and triangular waves using the AWG. The consistent measurement results presented in Fig. 4 provide evidence to support this claim.

The precision was achieved via 100-times acquisition, data transmission, and data processing, and it took approximately 1 s per cycle, with time being mainly consumed in the transmission part. When the OSC was replaced with a high-speed acquisition card, the system achieved 1000 LOS scans of output per second, and the fs-level precision was realized in 0.1 s.

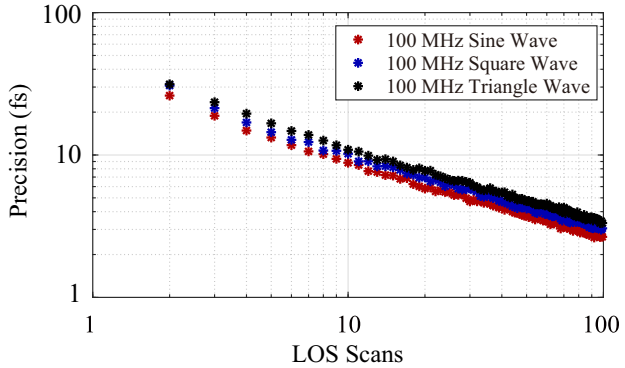

Fig. 4. Measurement precision (processed data) of the system using 100 MHz sine waves, square waves, and triangular waves. The result shows similar measurement precision for the different waveforms.

C. Key Parameters Analysis

To investigate the noises introduced by different components, we analyzed the key elements influencing our system's performance. The system's performance was limited by various factors, including the synchronization precision of combs A and B from the signal being tested, the amplitude noise from the detectors, and the sampling rate.

The amplitude noise and sampling rate affected the system precision during the localization process. To investigate their influence in detail, we simulated them with the LOS model described in the Appendix A. In our experiment, the BPD and the light source introduced amplitude noise with a standard deviation of 7 mV, which is approximately 1.32% of an LOS pulse, and we denote it as the relative intensity noise (RIN). The RIN affects the localization process and thus brings a fitting error to the measurement result, as shown in Fig. 5(a). We used 1.32% Gaussian white noise added on an LOS signal's amplitude to simulate the system's performance. The sampling rate was set to 500 MHz, as determined by the experimental parameters, and the standard deviation of the calculated time interval fluctuation was 19 fs [see Fig. 5(b)].

Note that the influence of the RIN was tightly connected, with both the f_{CEO} (carrier-envelope offset frequency; see the Appendix A) difference between the two combs of an LOS signal and the sampling rate of the OSC. Because the f_{CEO} of the combs are all free-running, it is crucial to choose an appropriate sampling rate to reduce the influences brought by the drift of the f_{CEO} and also consider the processing speed. For that purpose, we simulated the relation of the RIN-induced time fluctuation, the f_{CEO}-difference, and the sampling rate for a fixed RIN level 1.32%, and the results are shown in Fig. 5(c). The y axis ranges from 0 to 50 MHz because of the 100 MHz repetition frequency of the combs; a larger $\Delta f_{\mathrm{CEO}} = f_r/2 + \delta f$ is practically equivalent to $\Delta f_{\mathrm{CEO}} = f_r/2 - \delta f$ because of the periodicity of the combs' spectrum.

The results of Fig. 5(c) illustrate that when the sampling rate was larger than the repetition frequency (namely, 100 MHz),

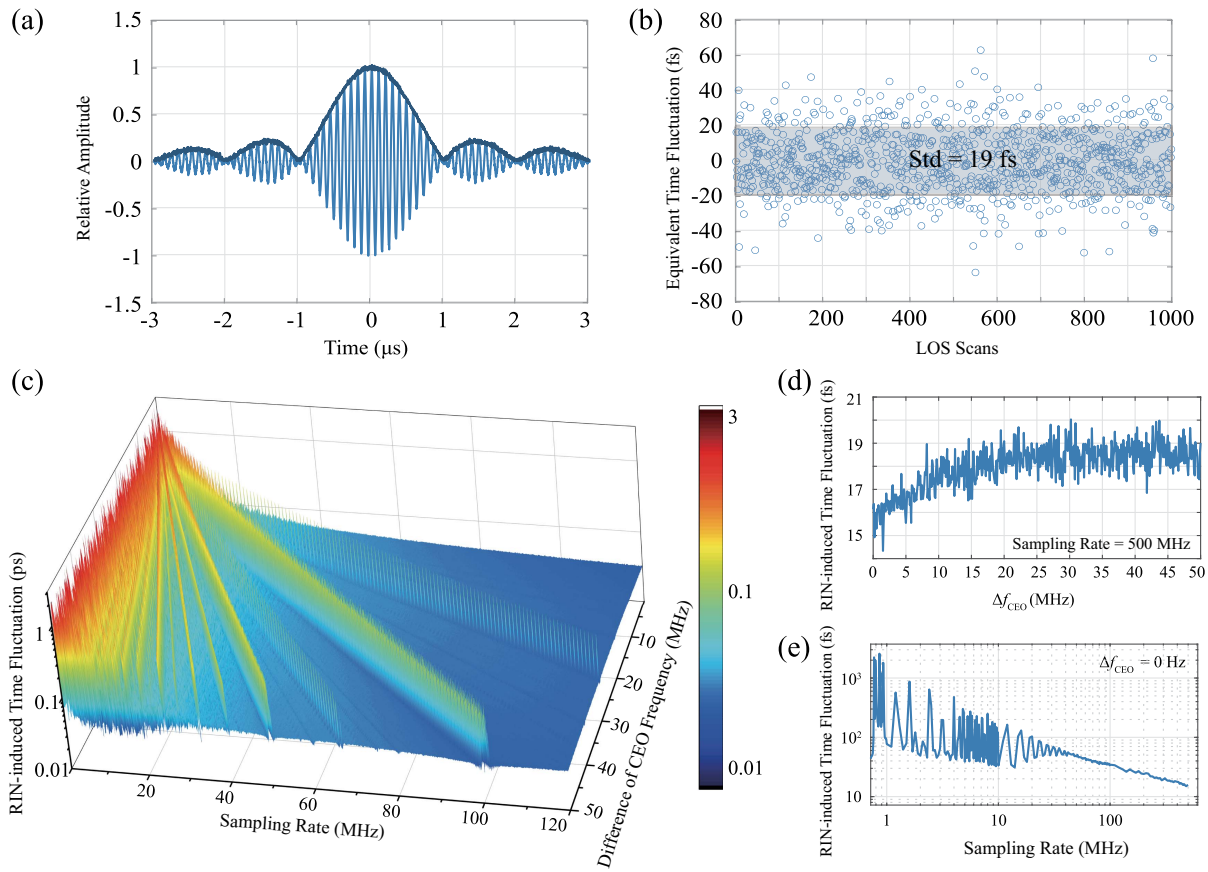

Fig. 5. Simulation results of the effect of the relative intensity noise (RIN)-induced time fluctuation. (a) The RIN affects the localization process and brings fitting errors. (b) The time fluctuation is caused by 1.32% RIN, where the sampling rate is set to 500 MHz corresponding to the experimental parameter. (c) The relation of RIN-induced time fluctuation, f_{CEO}-difference, and sampling rate for a fixed RIN level 1.32%. (d) The RIN-induced time fluctuation under the sampling rate of 500 MHz. (e) The RIN-induced time fluctuation under the f_{CEO}-difference of 0 Hz.

the RIN-induced time fluctuation was not evidently related to Δf_{CEO}. The higher the sampling rate is, the lower the noise that would remain. The 500 MHz sampling rate in our experiment led to 16–20 fs noise, as shown in Fig. 5(d), which is relatively low compared to the phase-locking-induced noise. If the sampling rate was below 100 MHz, the time interval fluctuation level would be affected because of the varying f_{CEO} of the combs. When the Δf_{CEO} was around a half-integer multiple of the sampling rate, the noise significantly increased because of the inaccurate sampling of the pulse. In addition, when the sampling rate fell lower, the noise level of other points also gradually increased because the amplitude fluctuation cannot be effectively averaged out with so few points. Moreover, to further improve the localization precision, increasing the optical bandwidth of the OF and equivalently decreasing the pulse width could potentially make a significant contribution.

According to the system's model given in the Appendix A, the measurement noise floor was mainly composed of the residual phase noise introduced by phase locking, and the RIN-induced time fluctuation, which is

$$\sigma_{\mathrm{floor}} = \sqrt{\sigma_{\mathrm{PL_A}}^2 + \sigma_{\mathrm{PL_B}}^2 + \sigma_{\mathrm{RIN_A}}^2 + \sigma_{\mathrm{RIN_B}}^2}, \tag{2}$$

where σ denotes the standard deviation of residual phase noise. The locking-induced noise was measured by $\sigma_{\mathrm{PL_A}} = \sigma_{\mathrm{PL_B}} = 45$ fs, and the RIN-induced noise was measured by $\sigma_{\mathrm{RIN_A}} = \sigma_{\mathrm{RIN_B}} = 19$ fs, which yielded a system noise floor of 69 fs. This calculated result indicates that the dominant noise in the existing system is locking-induced noise, which can be further optimized using a higher-order harmonic for the FLOM-PD's phase tracking. The experimentally measured noise floor of the system was 82 fs, which is consistent with the calculated result. The difference between the calculated noise floor and the measured noise floor may have stemmed from the fluctuation of the amplification parameter α caused by the small fluctuation of the DDS-generated frequency difference Δf_{r}.

Interestingly, in Fig. 5(c), for some fixed Δf_{CEO}, there were still low sampling rate regions with relatively low RIN-induced time fluctuations. For instance, if the Δf_{CEO} could be manually controlled to 0 Hz, the regions that have large noise (the green regions) could be avoided, even with low sampling

rates, as shown in Fig. 5(e). In this situation, the sampling rate of 100 MHz was sufficient to achieve RIN-induced noise below 40 fs (below the phase-locking-induced noise), although the system complexity would worsen. It is noteworthy that the oscillations observed in Figs. 5(d) and 5(e) are likely a result of the manually added Gaussian noise. Therefore, our focus lies in the overall magnitude rather than the specific values of individual data points.

For future studies, since the RIN-induced localization noise is at a relatively low level and has limited influence on the system performance at this stage, we did not conduct further in-depth research on this aspect and experimentally treated it as a known factor; the experimentally measured value is 1.32%. However, it is a complex composite consisting of at least analog–digital conversion quantization accuracy, detector electrical noise, and shot noise. It will be an important theoretical question to be analyzed and calculated after improving the accuracy of the light source locking.

In other aspects, the update rate (equal to Δf_r) is also a crucial consideration in some applications. It can be increased by simply enlarging Δf_r. However, it cannot be infinitely large, considering the LOS amplification factor α and the Nyquist bandwidth. Exploring the trade-off between these factors would be a valuable area for further research.

D. Discussion

In this study, with the optical mean (namely, the LOS technique), we achieved a high-precision and simple time interval measurement setup that can drastically promote the precise measurement of electrical signals. For demonstration, we built a CEO-free system to meaure the time interval of two squared electrical signals, and simulations were implemented to optimize the experimental parameters. Experimentally, we achieved 83 fs in a single-LOS-scan precision, and we further approached 3.05 fs with data processing, which is about three orders of magnitude better than the result of traditional time interval counter methods.

Compared to traditional direct detection of the time interval, our method has the advantage of avoiding the ambiguity brought by the rising edge of a pulse, creating the potential for the time interval measurement of arbitrary waveform pulsed signals. The possible restrictions of the performance were also discussed theoretically, and they can guide us toward further optimization of the setup. In our approach, the measurement is performed by synchronizing the combs with the periodic signals under test. As a result, we are currently unable to measure the time interval between individual pulses, and this aspect is left for future investigation. Based on our work, a real-time high-precision time interval measurement system can be developed to achieve sub-fs measurement, which we believe will open a new pathway for high-precision metrology, such as ultrahigh precision navigation and time synchronization.

APPENDIX A: METHODS

A. Basic Principles of the LOS Technique

The LOS technique is achieved by the interference between three OFCs, whose spectrum comprises a series of narrow bandwidth lines with the frequency f_n, which can be written as $f_n = f_{\mathrm{CEO}} + nf_r$, where n represents large integers (typically with the order of 10^6, with f_n being in an optical region). Moreover, f_r denotes the repetition frequency, and f_{CEO} is the carrier envelope offset (CEO) frequency, which is related to the carrier and envelope phase offset. In the time domain, a pulse train with a short duration and a period of $1/f_r$ is generated by an OFC, and the ultralow noise timing jitter is usually obtained by locking its phase to a reference oscillator. High time resolution measurement benefits from sampling one OFC signal with another OFC that has a slight repetition frequency offset Δf_r. The effective time measurement result is theoretically optimized by a magnifying factor $\alpha = f_r/\Delta f_r$. Specifically, the envelope phase variation of each comb is enlarged and revealed on the macroscopic signal with the relation

$$\Delta T = \alpha \Delta \tau, \tag{A1}$$

where ΔT is the phase time fluctuation of the LOS signal, which effectively stretches the time interval $\Delta\tau$ of the signal under test by α times in the time domain. Note that each LOS cycle consists of 100,000 pairs of comb pulses, and it requires reproducibility in both comb signals.

B. Comb

Self-developed SESAM-based OFCs are built with a 1560 nm central wavelength and 12 nm line width. The repetition frequency f_r is approximately 100 MHz, which is adjusted by a piezoelectric ceramic transducer (PZT) with a bandwidth of 100 Hz, an optical delay line with an adjustable range up to 1 MHz and a 100 Hz step, and a temperature-controlling plate with a 10 K temperature-controlling range and 0.001 K precision.

The OFCs have 100 mW of output power, which is achieved with a built-in erbium-doped fiber amplifier (EDFA). The high output power ensures that the energy is sufficient for the subsequent operations, including phase locking, interference, and monitoring. The polarization of the OFCs is stabilized with polarization controllers for the stability of the interference. The CEO frequency f_{CEO} of the combs does not need to be controlled, so the system complexity can be significantly reduced.

C. Signal Preprocessing

To achieve the fs precision time interval measurement, we expect the phase of the electrical signals being tested to be transferred to the corresponding OFCs precisely to employ the follow-up LOS technique; then, we can expect the interval of the combs to be stretched by LOS and precisely measured based on the combs' high time resolution characteristics. The signal preprocessing procedure aims to filter (together with multiplying/dividing) a single frequency component with no phase distortion, which can serve as the reference oscillator of combs A and B.

Assume that two arbitrary signals have the forms given by

$$s_{\mathrm{U1}}(t) = \sum_n g_1(t - nt_{\mathrm{U1}} - \tau_1), \tag{A2}$$

$$s_{\mathrm{U2}}(t) = \sum_n g_2(t - nt_{\mathrm{U2}} - \tau_2), \tag{A3}$$

where $g_1(t)$ and $g_2(t)$ are envelopes of two signals under test, t_{U1} and t_{U2} denote the periods of two signals, and τ_1 and τ_2

denote their phase times. The time interval under test is the phase-time difference (i.e., $\Delta\tau = \tau_1 - \tau_2$). When the signals with fixed delays under test have the same frequency, one can obtain the fixed values when measuring the phase time, the phase, and the delay between peaks. Moreover, it is important to note that when two signals with fixed delays have different frequencies, their phase time remains constant. However, a phase slip occurs when trying to determine the delay between two sets of peaks. To avoid ambiguity, it is more appropriate to use the phase time difference to represent the time interval of the periodic signals, rather than using the delay between peaks (or equivalently, the phase $2\pi f\tau$) directly. After the signals pass through the BPFs with the transfer function of $h_i(t)$ and $h_j(t)$, we can obtain the quasi-single frequency signals, given by

$$s_1(t) = s_{U1}(t) * h_i(t) = \sin[2\pi i f_{U1}(t - \tau_1)], \tag{A4}$$

$$s_2(t) = s_{U2}(t) * h_j(t) = \sin[2\pi j f_{U2}(t - \tau_2)], \tag{A5}$$

where the asterisk denotes convolution, i, j are integers quantifying the i-th and j-th harmonics of the measured signals, respectively, and $f_{U1} = 1/t_{U1}$ and $f_{U2} = 1/t_{U2}$ are the frequencies of the signals under test. To realize synchronization with the combs, the frequency of if_{U1} and jf_{U2} must be manually filtered and multiplied to be in the bandwidth of the locking system (i.e., near integer multiples of 100 MHz).

Note that for arbitrary waveform signals, different harmonics have different energies. For situations where direct filtering of the high-order harmonic is not feasible, an alternative approach is to obtain it by multiplying the first-harmonic signal, which typically possesses the highest energy. Furthermore, because the introduced time interval resulting from optical-microwave synchronization using FLOM-PD is unaffected by the power levels of the electrical signal, harmonic energy differences will not influence subsequent experiments. This characteristic enables our scheme to measure different waveform signals or use different frequency components without compromising the measurement results.

D. Conversion from Electrical to Optical Signals

To fully use the high time resolution characteristic of OFCs, we must ensure that the OFCs carry the time information of the electrical signals under test by phase-locking techniques. To realize high-precision phase locking, we use the FLOM-PDs, whose noise property surpasses the traditional mixer technique 38]]. The output of each OFC is split with a 50:50 beam splitter (BS), and the power of each arm is controllable with an optical attenuator. The branch used for phase-locking is set to 8 mW, ensuring sufficient energy of the error signal, and the one used for LOS interference is set to 20 mW so that the signal is large enough after the optical filter.

E. Data Acquisition and Post-Processing

For data processing, the LOS signals' envelopes $A_i(t)$ ($i = 1, 2$ is the signal number) carry the time information of the signals under test, so they are preliminarily extracted with the Hilbert transformation

$$A_i(t) = \mathcal{H}[s(t)] = h(t) * s(t) = \frac{1}{\pi}\int_{-\infty}^{\infty}\frac{s(\tau)}{t-\tau}\mathrm{d}\tau. \tag{A6}$$

Conventionally, the delay can be extracted with curve-fitting on the envelope and peak-finding, while the line shape of the LOS envelope depends on the OFCs' mode-locking process and needs optimization for different OFCs, such as hyperbolic secant fitting for an LOS signal generated by two soliton mode-locked lasers. If the gain narrowing effect of the amplifiers is considered, the line shape can be approximated to Gaussian [41]. In addition, the curve fitting is time-consuming, especially for a large data set. It is thus unfavorable for real-time processing of the data. Here, we use a more efficient and precise way; namely, we calculate the envelopes' center of gravity with the definition

$$t_i = \frac{\int_{-\infty}^{\infty} A_i(t') \times t'\mathrm{d}t'}{\int_{-\infty}^{\infty} A_i(t')\mathrm{d}t'}, \qquad i = 1, 2, \tag{A7}$$

where t' represents the time axis, and the result is shown in Fig. 2 with black dots. Repeating the process above, one can continuously measure the time differences in real time. To optimize the system precision, we designed a single-dimension Kalman filter to realize real-time processing of the time interval data and restrain the white noise induced by the localization process.

Additionally, a full scan of the LOS waveform covers multins oscillator time and most of it measures baseline. To improve the efficiency of our scheme, we implemented a threshold-based approach. If a data point is determined to be a baseline, instead of recording it, we increase the index of the data, thus optimizing the data processing speed in our implementation. Optimizing the measurement duty cycle would be another effective way, by using, e.g., time-programmable frequency combs [30]. We will leave this question for future studies.

F. System Model

To give a further explanation of our system, one can consider the signal of comb B and comb X in a specific optical channel (about 0.8 nm in width). Both combs are composed of $N = 1000$ comb teeth, and the fluctuations of their repetition frequency and CEO frequency are considered. The signal of comb B can be written as

$$\begin{aligned} &s_B(t - T) \\ &= \sum_{n=0}^{N-1}\cos\left\{\int_0^{t-T}\{[\omega_0^B + \delta\omega_0^B(t')] + n[\omega_r + \delta\omega_r^B(t')]\}\mathrm{d}t'\right\}, \\ &= \sum_{n=0}^{N-1}\cos\{(\omega_0^B + n\omega_r)(t - T) \\ &\quad + \int_0^{t-T}[\delta\omega_0^B(t') + n\delta\omega_r^B(t')]\mathrm{d}t'\}, \end{aligned} \tag{A8}$$

and, similarly, that of comb X can be written as

$$\begin{aligned} s_X(t) = \sum_{n=0}^{N-1}&\cos\{[\omega_0^X + n(\omega_r + \Delta\omega_r)]t \\ &+ \int_0^t[\delta\omega_0^X(t') + n\delta\omega_r^X(t')]\mathrm{d}t'\}, \end{aligned} \tag{A9}$$

where ω_0 and $\delta\omega_0(t)$ are the lowest angular frequency in the spectral channel and its fluctuation, respectively, which are determined by f_{CEO} and its fluctuation. ω_r and $\delta\omega_r(t)$ are the

repetition angular frequency and its fluctuation, respectively. $\Delta\omega_r$ is the repetition frequency offset, and N is the number of the comb teeth in the channel. Interfering in the coupler, the signal detected by the BPD is the multiplication of $s_B(t-T)$ and $s_X(t)$, i.e.,

$$\begin{aligned} I(t) &= s_B(t-T)\times s_X(t) \\ &= \sum_{n\Delta\omega_r<2\pi B}\cos\Bigg\{(\omega_0^X-\omega_0^B+n\Delta\omega_r) \\ &\quad\times\Bigg\{t+\frac{\omega_r}{\Delta\omega_r}\Bigg[T+\frac{1}{\omega_r}\int_0^t\delta\omega_r^X(t')\mathrm{d}t' \\ &\quad-\frac{1}{\omega_r}\int_0^{t-T}\delta\omega_r^B(t')\mathrm{d}t'\Bigg]\Bigg\} \\ &\quad+\int_0^t\delta\omega_0^X(t')\mathrm{d}t'-\int_0^{t-T}\delta\omega_0^B(t')+(\omega_0^X-\omega_0^B)\mathrm{d}t'\Bigg\} \\ &= \sum_{n\Delta\omega_r<2\pi B}\cos\Bigg\{(\Delta\omega_0+n\Delta\omega_r) \\ &\quad\times\Bigg\{t+\frac{\omega_r}{\Delta\omega_r}\Big[T+x^X(t)-x^B(t-T)\Big]\Bigg\} \\ &\quad+\varphi_0^X(t)-\varphi_0^B(t-T)\Bigg\}, \end{aligned} \tag{A10}$$

where $x(t)=\frac{1}{\omega_r}\int_0^t\delta\omega_r(t')\mathrm{d}t'$ is the phase time fluctuation induced by the repetition frequency fluctuation, $\varphi_0(t)=\int_0^t\delta\omega_0(t')\mathrm{d}t'$ indicates the phase noise induced by the frequency fluctuation of ω_0, and B is the bandwidth of BPD. From this result, one can see that the LOS signal has a similar form to a comb signal, and its repetition frequency is the repetition frequency offset of the two combs $\Delta\omega_r$. Moreover, the delay of the signal under test T and the phase time fluctuation induced by $\delta\omega_r(t)$ of both of the combs are enlarged by a factor of $\omega_r/\Delta\omega_r$. Considering the noise property, we determine the frequency stability of the LOS signal by both of the combs' repetition frequency stability. Statistically and precisely, because the two noise sources are independent of each other, one can write

$$\langle x^{\mathrm{LOS}}(t)\rangle=\frac{\omega_r}{\Delta\omega_r}\sqrt{\langle x^X(t)\rangle^2+\langle x^B(t)\rangle^2}. \tag{A11}$$

This means that the measured single LOS signal frequency stability is determined by the relative repetition frequency fluctuation of comb B, comb X, and the enlargement factor $(\omega_r/\Delta\omega_r)$.

Together with the LOS signal of comb X and comb A, the relative fluctuation of their phase time difference (that is, the system limit) can be written as

$$\langle x^T(t)\rangle=\frac{\omega_r}{\Delta\omega_r}\sqrt{\langle x^A(t)\rangle^2+\langle x^B(t)\rangle^2}, \tag{A12}$$

which indicates that the phase time fluctuation of comb X can be omitted on the condition that the difference in the delay from comb X to comb A and comb B can be omitted, which can be easily fulfilled.

In addition, from Eqs. (A8)–(A10), it is seen that the form of an LOS signal is exactly the same as that of a comb signal. Furthermore, $\Delta\omega_0$ of the LOS signal corresponds to ω_0 of a comb signal, which indicates that $\Delta\omega_0$ is the carrier frequency of the LOS signal and does not influence the envelopes' phase time. By contrast, intuitively, to ensure the localization precision, the system ensures that $\Delta\omega_0$ is intimately linked to the sampling rate. Based on the simple formula of Eq. (A8), we simulated the influence of $\Delta\omega_0$, the sampling rate, and RIN on the localization precision. The results are shown in Fig. 5.

Over and above that, Eq. (A8) is also a powerful tool to describe not only its own comb signal but also those affected by fiber dispersion and other nonlinear effects.

Funding. China Postdoctoral Science Foundation (2020TQ0016); National Natural Science Foundation of China (61531003, 62201012).

Author Contributions. All the authors contributed to the scientific discussions of the study. Z.C., B.L., and H.G. conceived the study. D.Y. and Z.C. developed the experimental plan. D.Y., Z.C., Y.X., Z.J., P.M., and Y.Z. designed, built, and experimentally validated the time interval measurement setup and performed the data analysis. S.Y., B.L., and H.G. discussed the optimization of the experiment scheme. D.Y. and X.Y. performed the data processing. D.Y. carried out the theoretical calculations and the simulation. D.Y. and Z.C. co-wrote the manuscript, and all authors provided revisions.

Disclosures. The authors declare no conflicts of interest.

Data Availability. Data underlying the results presented in this paper are not publicly available at this time but may be obtained from the authors upon reasonable request.

REFERENCES

1. Q. Shen, J.-Y. Guan, J.-G. Ren, T. Zeng, L. Hou, M. Li, Y. Cao, J.-J. Han, M.-Z. Lian, Y.-W. Chen, X.-X. Peng, S.-M. Wang, D.-Y. Zhu, X.-P. Shi, Z.-G. Wang, Y. Li, W.-Y. Liu, G.-S. Pan, Y. Wang, Z.-H. Li, J.-C. Wu, Y.-Y. Zhang, F.-X. Chen, C.-Y. Lu, S.-K. Liao, J. Yin, J.-J. Jia, C.-Z. Peng, H.-F. Jiang, Q. Zhang, and J.-W. Pan, "Free-space dissemination of time and frequency with 10^{-19} instability over 113 km," Nature **610**, 661–666 (2022).
2. J.-D. Deschênes, L. C. Sinclair, F. R. Giorgetta, W. C. Swann, E. Baumann, H. Bergeron, M. Cermak, I. Coddington, and N. R. Newbury, "Synchronization of distant optical clocks at the femtosecond level," Phys. Rev. X **6**, 021016 (2016).
3. M. Xin, K. Safak, and F. X. Kärtner, "Ultra-precise timing and synchronization for large-scale scientific instruments," Optica **5**, 1564–1578 (2018).
4. Q. Shen, J.-Y. Guan, T. Zeng, Q.-M. Lu, L. Huang, Y. Cao, J.-P. Chen, T.-Q. Tao, J.-C. Wu, L. Hou, S.-K. Liao, J.-G. Ren, J. Yin, J.-J. Jia, H.-F. Jiang, C.-Z. Peng, Q. Zhang, and J.-W. Pan, "Experimental simulation of time and frequency transfer via an optical satellite–ground link at 10^{-19} instability," Optica **8**, 471–476 (2021).
5. Y. Shen, S. Mazuelas, and M. Z. Win, "Network navigation: theory and interpretation," IEEE J. Sel. Areas Commun. **30**, 1823–1834 (2012).
6. J. Neil, L. Cosart, and G. Zampetti, "Precise timing for vehicle navigation in the smart city: an overview," IEEE Commun. Mag. **58**, 54–59 (2020).
7. B. Jaduszliwer and J. Camparo, "Past, present and future of atomic clocks for GNSS," GPS Solutions **25**, 27 (2021).

8. P. Zhang, R. Tu, X. Lu, Y. Gao, and F. Lihong, "Performance of global positioning system precise time and frequency transfer with integer ambiguity resolution," Meas. Sci. Technol. **33**, 045005 (2022).
9. Q. An, "Review of methods and techniques of precise time interval measurements for particle physics experiments," Nucl. Tech. **29**, 453–462 (2006).
10. B. M. Roberts, G. Blewitt, C. Dailey, M. Murphy, M. Pospelov, A. Rollings, J. Sherman, W. Williams, and A. Derevianko, "Search for domain wall dark matter with atomic clocks on board global positioning system satellites," Nat. Commun. **8**, 1195 (2017).
11. N. Huntemann, B. Lipphardt, C. Tamm, V. Gerginov, S. Weyers, and E. Peik, "Improved limit on a temporal variation of m_p/m_e from comparisons of Yb^+ and Cs atomic clocks," Phys. Rev. Lett. **113**, 210802 (2014).
12. A. Derevianko and M. Pospelov, "Hunting for topological dark matter with atomic clocks," Nat. Phys. **10**, 933–936 (2014).
13. J. Liu, X. Chen, and X. Ji, "Current status of direct dark matter detection experiments," Nat. Phys. **13**, 212–216 (2017).
14. J. C. Berengut and V. V. Flambaum, "Testing time-variation of fundamental constants using a 229th nuclear clock," Nuclear Phys. News **20**, 19–22 (2010).
15. M. Safronova, D. Budker, D. DeMille, D. F. J. Kimball, A. Derevianko, and C. W. Clark, "Search for new physics with atoms and molecules," Rev. Mod. Phys. **90**, 025008 (2018).
16. Y. V. Stadnik and V. V. Flambaum, "Searching for dark matter and variation of fundamental constants with laser and maser interferometry," Phys. Rev. Lett. **114**, 161301 (2015).
17. K. Józef, "Review of methods for time interval measurements with picosecond resolution," Metrologia **41**, 17 (2004).
18. I. P. Dan, "Review of sub-nanosecond time-interval measurements," IEEE Trans. Nucl. Sci. **20**, 36–51 (1973).
19. J. Zhao, Z. Zhao, and L. Fu, "Research on the high resolution precision time-interval measurement methods," Proc. Eng. **174**, 1257–1261 (2017).
20. S. Henzler, *Time-to-Digital Converter Basics* (Springer, 2010).
21. X. Ren and X. F. Zhang, "Methods of high precision time-interval measurement," in *4th International Conference on Electronic Information Technology and Computer Engineering (EITCE)* (2020).
22. J. P. Jansson, A. Mantyniemi, and J. Kostamovaara, "A CMOS time-to-digital converter with better than 10 ps single-shot precision," IEEE J. Solid-State Circuits **41**, 1286–1296 (2006).
23. D. W. Allan and H. Daams, "Picosecond time difference measurement system," in *Symposium on Frequency Control* (1975).
24. N. R. Newbury, "Searching for applications with a fine-tooth comb," Nat. Photonics **5**, 186–188 (2011).
25. J. L. Hall, "Nobel lecture: defining and measuring optical frequencies," Rev. Mod. Phys. **78**, 1279–1295 (2006).
26. H. Margolis, G. Barwood, G. Huang, H. Klein, S. Lea, K. Szymaniec, and P. Gill, "Hertz-level measurement of the optical clock frequency in a single $^{88}Sr^+$ ion," Science **306**, 1355–1358 (2004).
27. S. A. Diddams, T. Udem, J. Bergquist, E. Curtis, R. Drullinger, L. Hollberg, W. M. Itano, W. Lee, C. Oates, and K. Vogel, "An optical clock based on a single trapped $^{199}Hg^+$ ion," Science **293**, 825–828 (2001).
28. H. Bergeron, L. C. Sinclair, W. C. Swann, I. Khader, K. C. Cossel, M. Cermak, J.-D. Deschênes, and N. R. Newbury, "Femtosecond time synchronization of optical clocks off of a flying quadcopter," Nat. Commun. **10**, 1819 (2019).
29. Q. Lu, Q. Shen, J. Guan, M. Li, J. Chen, S. Liao, Q. Zhang, and C. Peng, "Sensitive linear optical sampling system with femtosecond precision," Rev. Sci. Instrum. **91**, 035113 (2020).
30. E. D. Caldwell, L. C. Sinclair, N. R. Newbury, and J.-D. Deschenes, "The time-programmable frequency comb and its use in quantum-limited ranging," Nature **610**, 667–673 (2022).
31. M. Kajima and K. Minoshima, "A simple optical-zooming positioning system using a femtosecond frequency comb," in *Conference on Lasers & Electro-Optics* (2009).
32. M. Kajima and K. Minoshima, "Optical zooming interferometer for sub-nanometer positioning using an optical frequency comb," Appl. Opt. **49**, 5844–5850 (2010).
33. I. Coddington, W. C. Swann, L. Nenadovic, and N. R. Newbury, "Rapid and precise absolute distance measurements at long range," Nat. Photonics **3**, 351–356 (2009).
34. G. Marra, "Transfer of optical frequency combs over optical fibre links," Thesis (University of Southampton, 2013).
35. W. Zhang, T. Li, M. Lours, S. Seidelin, G. Santarelli, and Y. L. Coq, "Amplitude to phase conversion of InGaAs pin photo-diodes for femtosecond lasers microwave signal generation," Appl. Phys. B **106**, 301–308 (2012).
36. Z. Jin, Y. Xu, D. Yu, B. Luo, Z. Chen, G. Wu, and H. Guo, "Analyzing the influence of InGaAs photodetectors in comb-based frequency transfer," in *Frontiers in Optics + Laser Science* (2022).
37. J. Kim, F. X. Kärtner, and M. H. Perrott, "Femtosecond synchronization of radio frequency signals with optical pulse trains," Opt. Lett. **29**, 2076–2078 (2004).
38. K. Jung and J. Kim, "Subfemtosecond synchronization of microwave oscillators with mode-locked Er-fiber lasers," Opt. Lett. **37**, 2958–2960 (2012).
39. J. Kim, J. A. Cox, J. Chen, and F. X. Kärtner, "Drift-free femtosecond timing synchronization of remote optical and microwave sources," Nat. Photonics **2**, 733–736 (2008).
40. F. R. Giorgetta, W. C. Swann, L. C. Sinclair, E. Baumann, I. Coddington, and N. R. Newbury, "Optical two-way time and frequency transfer over free space," Nat. Photonics **7**, 434–438 (2013).
41. G. P. Agrawal, *Nonlinear Fiber Optics* (Springer, 2000).